Journal of Biomedical Optics

BiomedicalOptics.SPIEDigitalLibrary.org

Analysis of the change in peak corneal temperature during excimer laser ablation in porcine eyes

Samuel Arba Mosquera
Shwetabh Verma

SPIE.

Analysis of the change in peak corneal temperature during excimer laser ablation in porcine eyes

Samuel Arba Mosquera* **and Shwetabh Verma**
SCHWIND eye-tech-solutions, Mainparkstr. 6-10, Kleinostheim, Bavaria D-63801, Germany

Abstract. The objective is to characterize the impact of different ablation parameters on the thermal load during corneal refractive surgery by means of excimer laser ablation on porcine eyes. One hundred eleven ablations were performed in 105 porcine eyes. Each ablation was recorded using infrared thermography and analyzed mainly based on the two tested local frequencies (40 Hz, clinical local frequency; 1000 Hz, no local frequency). The change in peak corneal temperature was analyzed with respect to varying ablation parameters [local frequency, system repetition rate, pulse energy, optical zone (OZ) size, and refractive correction]. Transepithelial ablations were also compared to intrastromal ablations. The average of the baseline temperature across all eyes was 20.5°C ± 1.1 (17.7°C to 22.2°C). Average of the change in peak corneal temperature for all clinical local frequency ablations was 5.8°C ± 0.8 ($p = 3.3E-53$ to baseline), whereas the average was 9.0°C ± 1.5 for all no local frequency ablations ($p = 1.8E-35$ to baseline, 1.6E – 16 to clinical local frequency ablations). A logarithmic relationship was observed between the changes in peak corneal temperature with increasing local frequency. For clinical local frequency, change in peak corneal temperature was comparatively flat ($r^2 = 0.68$ with a range of 1.5°C) with increasing system repetition rate and increased linearly with increasing OZ size ($r^2 = 0.95$ with a range of 2.4°C). Local frequency controls help maintain safe corneal temperature increase during excimer laser ablations. Transepithelial ablations induce higher thermal load compared to intrastromal ablations, indicating a need for stronger thermal controls in transepithelial refractive procedures. [DOI: 10.1117/1.JBO.20.7.078001]

Keywords: thermal load; ocular surface temperature; excimer laser ablations; local and system frequency; optical zone; pulse energy; refractive correction; transepithelial ablations; intrastromal ablations; porcine cornea; temperature rise; denaturation; repetition rate.

Paper 140844R received Dec. 19, 2014; accepted for publication May 29, 2015; published online Jul. 2, 2015.

1 Introduction

Laser-based refractive surgery techniques are constantly being developed with a common aim of optimizing the surgery outcomes in terms of visual acuity, contrast sensitivity and night vision. Sophisticated algorithms and technological advancements help realize new features in refractive surgery like shorter treatment times, distributed thermal load with optimized spot patterns,[1,2] calibration systems,[1,3] precise eye tracking, and optimized ablation efficiency at non-normal incidence.[4,5] Spatial distribution of laser pulses on the cornea is controlled such that each pulse sequentially ablates a small amount of corneal tissue, collectively etching a very refined pattern calculated and designed to counterbalance the aberrations. Ultraviolet (UV) radiation commonly used in laser refractive surgeries is regarded as "cold" radiation. The reason for this consideration is that the thermal relaxation time of the molecules is usually shorter than the thermal denaturation time.[6] However, even these UV laser pulses also impart a certain thermal load to the cornea tissue seen as an increase in ocular surface temperature (OST), observed clinically[7–9] as well as in laboratory settings.[10,11] Furthermore, smaller laser spots are used along with the higher system repetition rates controlling the treatment time in most modern refractive surgery systems; each of these factors could impact the thermal response of the corneal tissue individually and in combination with other factors.

Heat that is gained from blood is conducted across the ocular media and is transferred into the environment from the corneal surface via convection and radiation. Parameters such as ambient temperature and convection heat transfer coefficient affect the heat loss from the corneal surface.[12] Contact thermometry is nowadays replaced by noninvasive infrared (IR) thermography. Thermography, however, does not measure temperature directly, but measures radiation intensity from which temperature is calculated. This means that parameters such as spatial, temporal and temperature resolution, field of view, angle of observation, the calibration of the apparatus, and the shielding against stray-radiation may influence the accuracy of the result. The emissivity of the emitting surface is highly important. In the absence of a tear film, the determined temperature is considered from the cornea.[13]

The use of IR thermography in ophthalmology was pioneered by Mapstone through a series of experiments published in 1968.[14–17] The uncertainty in temperature measurements in porcine cornea due to emissivity errors[18] and camera angle[19] has been previously reported. Commercially available thermography imaging systems featuring much greater system time constants, have been used for the evaluation of mean and maximum temperature rise within an ablated area.[20] Kim et al.[21] studied the expression patterns of heat shock proteins following eyeball heating or cooling in relation to corneal wound healing and

*Address all correspondence to: Samuel Arba Mosquera, E-mail: samuel.arba.mosquera@eye-tech.net

intraocular complications after excimer laser treatment. They were able to demonstrate that heat shock proteins were induced by thermal preconditioning and appeared to be a major factor in corneal protection against serious thermal damage.

Ishihara et al.[8] showed that the transient surface temperature of the cornea during ablation was much higher than previously reported, with thermal radiation from the surface of porcine corneas during ArF excimer laser irradiation showing a temperature over 100°C at a fluence of 80 mJ/cm^2 and of 240°C at a fluence of 180 mJ/cm^2.

Maldonado-Codina et al.[22] investigated the temperature changes occurring during photorefractive keratectomy (PRK) in 19 bovine corneas when performed at different ablation depths using noncontact, color-coded ocular thermography. They observed an average temperature rise of 8°C at the corneal surface with a maximum rise of 9°C. They found a positive correlation between the refractive correction and the peak temperature rise. De Ortueta et al.[23] evaluated the thermal load of ablation in high-speed laser corneal refractive surgery with the AMARIS excimer laser (SCHWIND eye-tech-solutions). They found that, overall, the maximum temperature change of the ocular surface induced by the refractive ablations was ≤4°C. The increase in the peak temperature of the ocular surface never exceeded 35°C in any case. This low-thermal load was independent of the amount of correction the eye achieved. Vetrugno et al.[24] reported that "high-repetition-rate excimer laser systems require spot sequences with optimized temporal and spatial spot distribution to minimize the increase in OST." Wernli et al.[25] evaluated the effects of initial surface temperature of poly-methyl-methacrylate (PMMA) plates used for daily laser calibration. They found that the ablation depth increased linearly from 73.9 to 96.3 μm within a temperature increase from 10.1°C to 75.7°C (increase rate of 0.3192 μm/K). The linear correlation was found to be significant ($P < 0.05$) with a coefficient of determination of $R^2 = 0.95$.

The average OST in humans has been reported to be approximately 34°C.[26–29] In clinical settings, where the globe is exposed using a lid speculum, a decrease of 3 to 4°C is expected in the corneal surface temperature.[23] At temperatures above 40°C, thermal damage of the corneal tissue may occur.[30] Assuming these metrics, the change in peak corneal temperature shall be maintained at best below 6°C, and definitely below 10°C, during the excimer laser ablation. If this thermal load is not controlled, it may lead to denaturation of the collagen proteins inducing thermal damage.[11,30,31]

Minimizing the thermal load of ablation in high-speed laser corneal refractive surgery has been analyzed theoretically and clinically in the past, in PMMA, porcine as well as human cornea, generating several models[11,20,32–34] for temperature increase during laser ablation. However, the real impact of the thermal load in laser corneal refractive surgery is still controversially discussed and warrants further in-depth exploration, particularly for high-repetition-rate scanning-spot excimer laser applications. The impacts of certain system and ablation parameters such as local frequency, system repetition rate, pulse energy, optical zone (OZ) size, and refractive correction, have not been individually and extensively analyzed in the light of an increase in optical surface temperature. Our aim with this work is to quantify and analyze the impact of these parameters on the increase in peak corneal temperature during "fast repetition rate" excimer laser ablation in porcine eyes, while using a flying spot algorithm to control the thermal load on the cornea. To these tested parameters, we analyzed the thermal impact of transepithelial ablations in comparison to stromal ablations. We used noninvasive IR thermography with a fast acquisition rate to record each ablation.

2 Methods

All the ablations were performed on *ex vivo* porcine eyes within five hours of procuring the eyes. The porcine eyes were stored in glucose solution (1L saline solution +19 ml of Dulbecco's Modified Eagle Medium low glucose solution from PAA Laboratories GmbH) at room temperature (~23°C), during transportation and before ablation. Every eye was mounted on a holder and was recorded with a thermal camera during ablation. A customized AMARIS laser system (SCHWIND eye-tech-solutions, Kleinostheim, Germany) allowing for manipulation of ablation parameters was used for performing the ablations with only a single fluence. The treatment plane was calibrated to the corneal vertex with the help of a slit lamp from the laser system. The impact of system and ablation parameters such as local frequency, system repetition rate, pulse energy, OZ, and refractive correction were analyzed, with only one parameter varied at a time. The system and ablation specifications for each test setting are presented in Table 1. For most of the ablations, the eyes were de-epithelized manually prior to ablation (using an Amoils brush). However, to analyze the role of epithelium in temperature control, items 32 and 34 (in Table 1) were each ablated on porcine eyes with natural epithelium. Each item in the Table 1 was repeated in three different eyes to analyze repeatability; additionally, *a* and *b* in items 33 and 35 represent consecutive ablations performed in the same eye (one on top of the other after a time gap of ~90 s) to analyze the thermal response of the outer and comparatively deeper stromal layers. The ablations represented with *a* and *b* had identical ablation parameters. The items 33 ($a + b$) and 35 ($a + b$) were also repeated in three different eyes. Therefore, items 32 and 34 analyzed the corneal thermal response to transepithelial ablations, items 33 and 35 (*a*) analyzed the corneal thermal response to first stromal ablations (closer to the corneal surface) while items 33 and 35 (*b*) analyzed the corneal thermal response to second stromal ablations (starting at deeper layers within the same eye). The second stromal ablation was performed ~128 μm (nominal depth of the treated correction of −9 D with an OZ 6.3 mm) deeper than the first stromal layer. It must be noted that with the first stromal ablation (33*a* and 35*a*), the nominal ablation depth of ~128 μm was achieved only in the center. In order to bring the periphery in level with the center (within the OZ) and achieve a flat stromal bed, before the second stromal ablation, the cornea was first ablated with a +8 D hyperopic profile (with no ablation at the center and ~128-μm ablation at the periphery). Subsequently, the second stromal ablation was performed (represented by 33*b* and 35*b* in Table 1) on a relatively flat stromal bed.

The customized AMARIS laser system used in our tests allowed for manipulation of ablation parameters like system repetition rates with or without the local ablation frequency controls. The system repetition rate of the laser system was set at 1050 Hz for most of the tests. The local frequency of 40 Hz in Table 1 represents the system repetition rate limited to the "intelligent thermal effect control" frequency[33] (normal iTEC frequency) of the AMARIS platform (i.e., system repetition rate limited to 40 Hz local ablation frequency), whereas the 1000-Hz local frequency represents essentially no local frequency

Table 1 System and ablation parameters. Each item was repeated in three different porcine eyes. Further, *a* and *b* in items 33 and 35 represent consecutive ablations in the same eye. Items 32 and 34 were each ablated on three different porcine eyes with natural epithelium. The rest of the ablations were performed on manually deepithilialized eyes (Amoils brush). For all the ablations, nonwavefront guided aspheric profiles were used, calculated for a vertex distance of 12 mm and keratometric readings (K1 and K2) of 44 D.

Item No.	System repetition rate (Hz)	Refractive correction (D)	Ablation depth (μm)	Optical zone (mm)	Local frequency (Hz)	Pulse energy (mJ)
			Local frequency			
1	1050	−9.0	128.2	6.3	40	1.33
2	1050	−9.0	128.2	6.3	1000	1.33
3	1050	−9.0	128.2	6.3	10	1.33
			System repetition rate			
4	1050	−9.0	128.2	6.3	40	1.33
5	1050	−9.0	128.2	6.3	1000	1.33
6	750	−9.0	128.2	6.3	40	1.33
7	750	−9.0	128.2	6.3	1000	1.33
8	500	−9.0	128.2	6.3	40	1.33
9	500	−9.0	128.2	6.3	1000	1.33
			Optical zone size			
10	1050	−9.0	53.0	4.0	40	1.33
11	1050	−9.0	53.0	4.0	1000	1.33
12	1050	−9.0	128.2	6.3	40	1.33
13	1050	−9.0	128.2	6.3	1000	1.33
14	1050	−9.0	166.0	7.5	40	1.33
15	1050	−9.0	166.0	7.5	1000	1.33
			Pulse energy			
16	1050	−9.0	128.2	6.3	40	1.33
17	1050	−9.0	128.2	6.3	1000	1.33
18	1050	−9.0	128.2	6.3	80	0.67
19	1050	−9.0	128.2	6.3	1000	0.67
			Refractive correction			
20	1050	−9.0	136.3	6.5	40	1.33
21	1050	−6.0	90.6	6.5	40	1.33
22	1050	−3.0	45.0	6.5	40	1.33
23	1050	+2.0	32.0	6.5	40	1.33
24	1050	+4.0	69.6	6.5	40	1.33
25	1050	+6.0	111.6	6.5	40	1.33
26	1050	−9.0	136.3	6.5	1000	1.33
27	1050	−6.0	90.6	6.5	1000	1.33
28	1050	−3.0	45.0	6.5	1000	1.33
29	1050	+2.0	32.0	6.5	1000	1.33
30	1050	+4.0	69.6	6.5	1000	1.33
31	1050	+6.0	111.6	6.5	1000	1.33

Table 1 (*Continued*).

Item No.	System repetition rate (Hz)	Refractive correction (D)	Ablation depth (μm)	Optical zone (mm)	Local frequency (Hz)	Pulse energy (mJ)
			Effect of epithelium			
32	1050	−9.0	128.2	6.3	40	1.33
33*a*	1050	−9.0	128.2	6.3	40	1.33
33*b*	1050	−9.0	128.2	6.3	40	1.33
34	1050	−9.0	128.2	6.3	1000	1.33
35*a*	1050	−9.0	128.2	6.3	1000	1.33
35*b*	1050	−9.0	128.2	6.3	1000	1.33

for the 1050 Hz (and lower) system repetition rate, with almost every pulse (9 out of 10 pulses) delivered with 1050-Hz frequency and minimal pulses (1 out of 10 pulses) delivered with 525-Hz frequency. These local frequency settings are represented here with the terms "clinical local frequency" (for 40 Hz) and "no local frequency" (for 1000 Hz), respectively. The "no local frequency" of 1000 Hz (in Table 1) should be considered as the maximum allowed frequency of the laser system. In addition to the system repetition rate of 1050 Hz, we also tested the impact of two additional system repetition rates (500 Hz and 750 Hz) with and without the local frequency controls (lines 4 to 9 in Table 1). In these cases (cases 7 and 9 in Table 1), "no local frequency," although set at 1000 Hz, actually means the highest achievable system repetition rate of the laser system (500 Hz and 750 Hz, respectively).

The change in local frequency did not affect the pulse energy in our test laser system. However, as a feature of our test software, under the influence of local frequency control, a change in laser pulse energy manipulated the local frequency in order to maintain a constant fluence received by the eye per unit of time. This control was deactivated for "no local frequency." Therefore, in cases 16 and 18 (Table 1), manipulation of pulse energy resulted in a change in local frequency. However, in cases 17 and 19 "no local frequency" was maintained (i.e., maximum allowed system frequency) even though the pulse energy was manipulated. We discuss the implication of these features in later sections.

Collectively, 105 eyes received 111 ablations in total. For all the ablations, nonwavefront guided aspheric ablation profiles were calculated for a vertex distance of 12 mm and keratometric readings (K1 and K2) of 44 D using the SCHWIND custom ablation manager (SCHWIND eye-tech-solutions, Kleinostheim, Germany). All the ablations were based on a pseudorandom algorithm with the local frequency controls implemented as described elsewhere.[34]

An IR thermal camera (FLIR-A 615) with a macro-objective was positioned at 10 cm distance from the ablation focus and was tilted horizontally to an angle of ~60 deg. Every ablation was recorded at 200 fps in windowed mode (~83 μm/pixel) with a centered elliptical window (region of interest) approximately 10 mm in size (at the major axis). The region of interest was specified manually and selected such that it covered the cornea completely and tightly enough that the variability between the porcine eyes could be accounted for. Therefore, some intact cornea was also analyzed around the OZ. The camera angle was manually adjusted before the experiment to completely cover the eyeball in the windowed mode. The region of interest and the camera angle were neither shifted nor adjusted throughout the experiment. Using the camera software, the measurements were internally adjusted for the recording distance, and emissivity was set at 0.9 in agreement to the literature.[20] With our test setup, we can expect a measurement error of ±0.5°C due to the thermal camera.[20] The pixel with the highest recorded temperature within the region of interest was analyzed. The baseline maximum temperature before starting the ablation and the peak of the maximum temperature achieved during the entire ablation were analyzed manually from the graphical representation of the maximum temperature (Fig. 1) achieved during the video recordings. Two such example video recordings are presented here (Fig. 2 with clinical local frequency, Fig. 3 with no local frequency). The change in peak corneal temperature was calculated from the difference of the two recorded values, the peak of the maximum temperature achieved during the entire ablation and the baseline maximum temperature before the ablation. Figure 1 presents an example with clinical local frequency, with a baseline maximum temperature of 20.8°C, peak of the maximum temperature 25.8°C and change in peak corneal temperature 5°C.

Data analysis was performed using Microsoft Excel (Microsoft Corporation). Correlation and paired single tailed *t*-tests were performed to analyze the differences among datasets with a 0.05 level of statistical significance. For curve fitting, we took an exploratory approach of maximizing the coefficient of determination (r^2 values).

3 Results

The maximum baseline temperature across all the ablated eyes was on an average 20.5°C ± 1.1 (17.7°C to 22.2°C). The change in peak corneal temperature for the ablations performed with clinical local frequency was on an average 5.8°C ± 0.8 ($p = 3.3\text{E}-53$ to baseline); whereas 9.0°C ± 1.5 was the average for the ablations performed with no local frequency ($p = 1.8\text{E}-35$ to baseline, $1.6\text{E}-16$ to clinical local frequency ablations). We analyzed the impact of each of the varying parameters on the change in peak corneal temperature.

3.1 *Local Frequency*

Three local frequency controls (10, 40, and 1000 Hz) were tested with a system repetition rate of 1050 Hz. The change in peak corneal temperature progressed logarithmically with respect to the increasing local frequencies (Fig. 4), with statistically significant differences among all the three tested local frequencies maximizing between clinical and no local

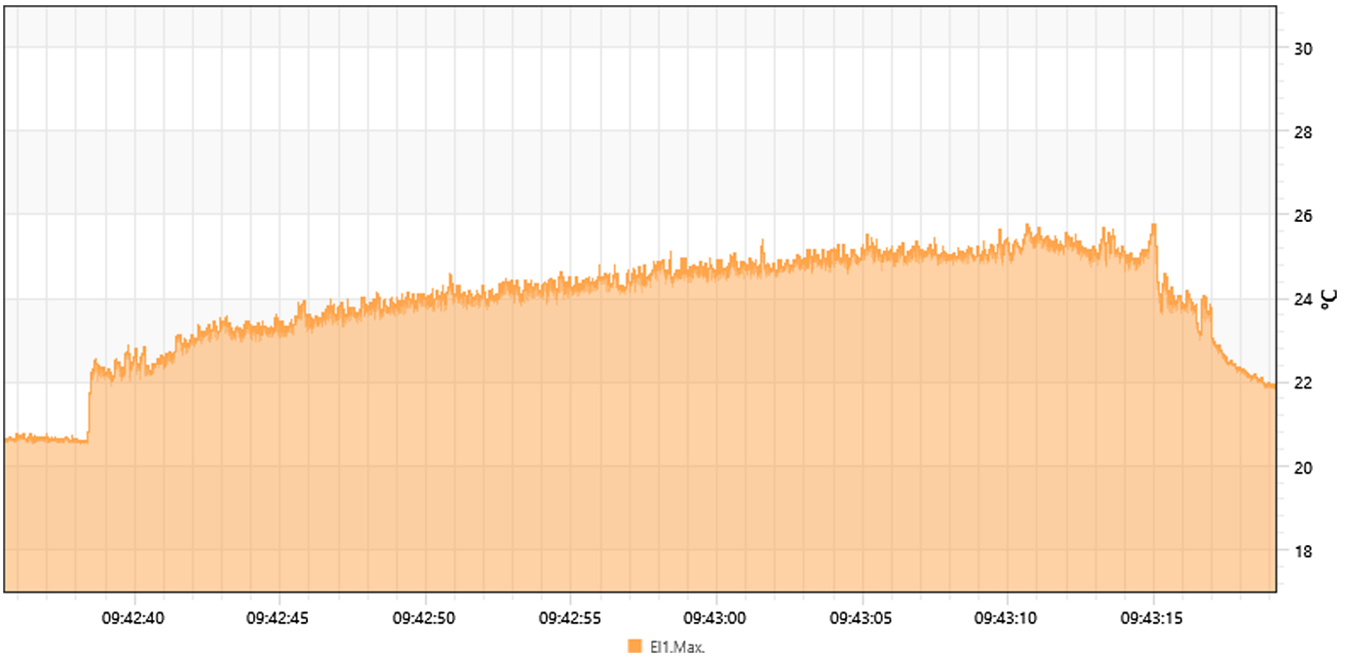

Fig. 1 A screenshot from the video recording with the thermal camera for the first ablation performed with the clinical local frequency for a refractive correction of −9 D with 6.3-mm OZ. The baseline and peak corneal temperature were recorded at 20.7°C and 25.8°C, respectively.

frequency ($p = 0.005$) (Table 2). For the clinical local frequency, the highest change in peak corneal temperature of 5.8°C was observed versus 11°C for no local frequency and 2.7°C for 10-Hz local frequency.

3.2 *Repetition Rate*

Three different system repetition rates (500, 750, and 1050 Hz) were tested with clinical and no local frequency controls. For the clinical local frequency, the measurements at 500 and 750 Hz system repetition rate were similar ($p = 0.3$) in comparison to 1050 Hz ($p < 0.02$) (Table 3). However, for no local frequency, measurements at all the tested repetition rates differed significantly ($p < 0.04$), increasing rapidly with the repetition rate (Fig. 5). The differences between the two local frequencies became more significant with increasing repetition rate ($p = 0.003$ for 1050-Hz system frequency). For the clinical local frequency, the maximum change in peak corneal temperature was

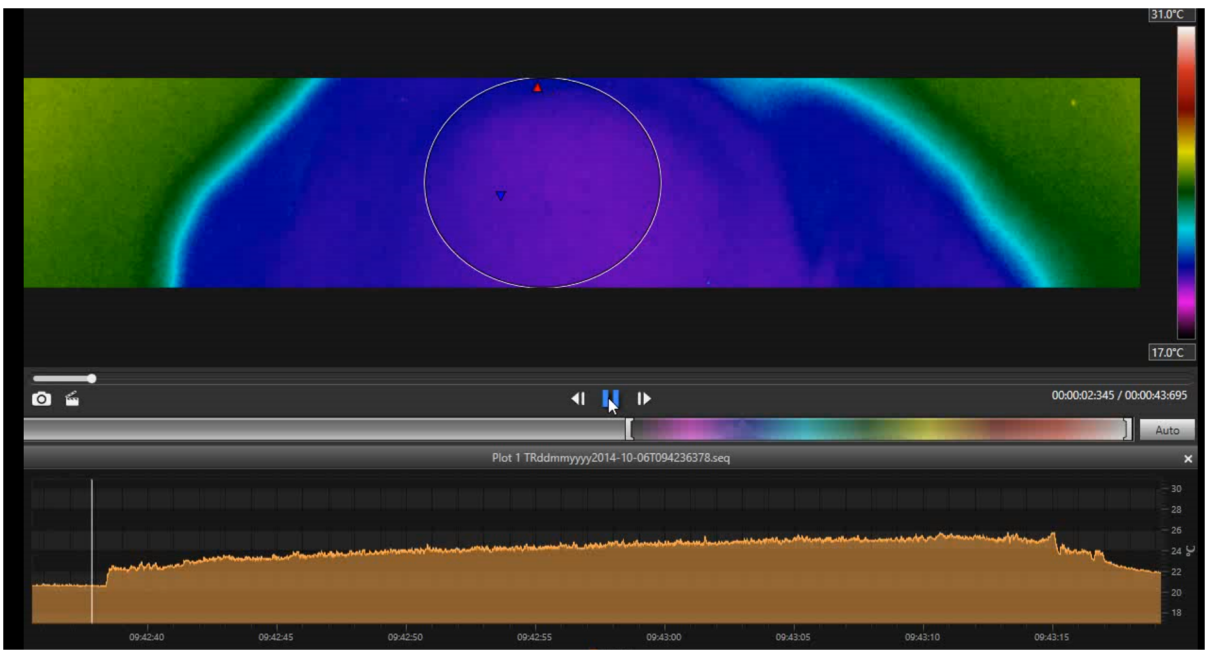

Fig. 2 An example ablation recording with clinical local frequency (Video 1, MOV, 5.2 MB) [URL: http://dx.doi.org/10.1117/1.JBO.20.7.078001.1].

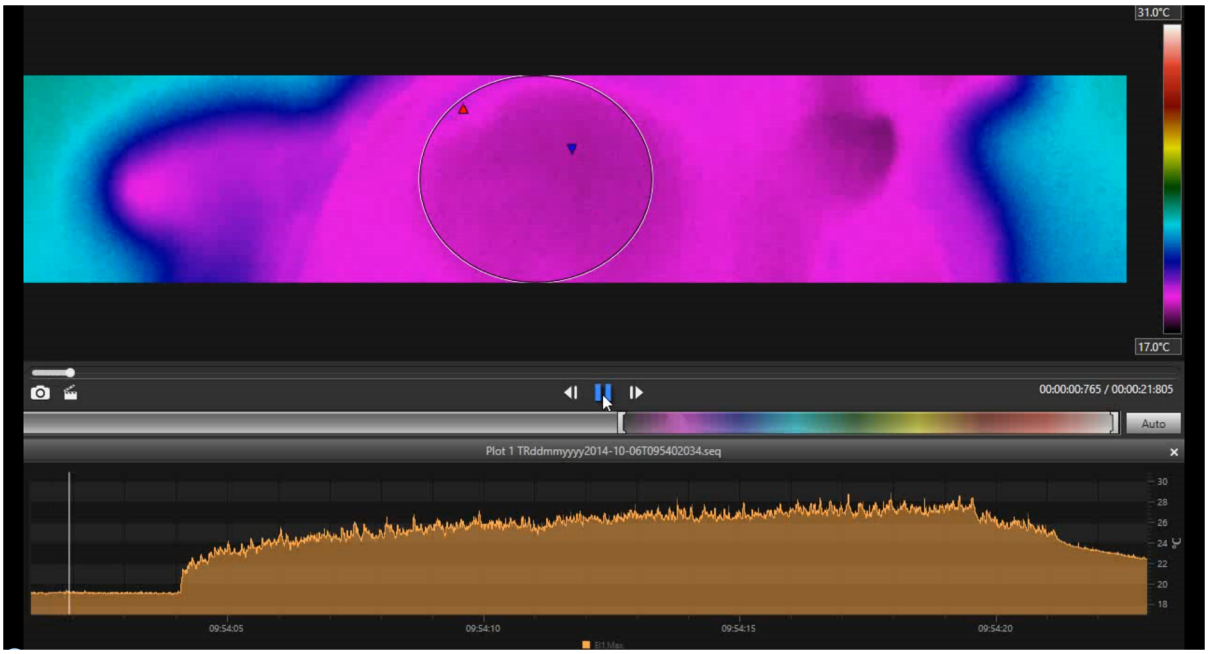

Fig. 3 An example ablation recording with no local frequency (Video 2, MOV, 2.93 MB) [URL: http://dx.doi.org/10.1117/1.JBO.20.7.078001.2].

limited to 6.8°C for the entire range of system repetition rates, however, reaching as high as 11°C for no local frequency.

3.3 *Optical Zone*

Three different OZs (4, 6.3, and 7.5 mm) were tested with clinical and no local frequency controls. For both clinical and no local frequencies, the differences between all the three OZs were statistically significant ($p < 0.02$) (Table 4). The paired t-test shows higher significant differences between the two local frequencies for 4 mm ($p = 0.0001$) and 7.5 mm ($p = 0.0002$) OZ compared to 6.3 mm (0.003). However, the progression with respect to the OZ shows a converging trend between the two local frequencies (Fig. 6) for wider OZs, with the change in peak corneal temperature increasing with the OZ for clinical local frequency while it decreased for no local frequency. For the clinical local frequency, the highest change in peak corneal temperature was limited to 6.6°C for the entire range of OZ, however, it reached as high as 12.1°C for no local frequency.

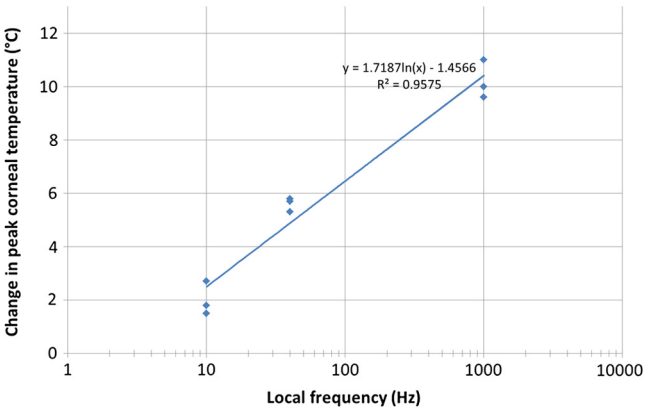

Fig. 4 The peak corneal temperature increased logarithmically with the increasing local frequency. However, for the clinical local frequency, the maximum change in peak corneal temperature was 5.8°C.

3.4 *Pulse Energy*

Two single pulse energy levels were tested (0.67 and 1.33 mJ). The clinical local frequency of 40 Hz was maintained for 1.33 mJ pulse energy, but for half of the pulse energy, the

Table 2 Thermal response to changing local frequency; for system repetition rate 1050-Hz, pulse energy 1.33 mJ, and optical zone (OZ) size 6.3 mm.

Local frequency (Hz)	Average change in peak temperature (°C)
10	2.0 ± 0.6
40	5.6 ± 0.3
1000	10.2 ± 0.7
p-value	0.005

Table 3 Thermal response to changing repetition rate. For both local frequencies, significant differences were observed between repetition rates, compared to 1050-Hz repetition rate. For all repetition rates, measurements at clinical local frequency were significantly lower versus no local frequency, with differences becoming more significant with increasing repetition rate.

Repetition rate (Hz)	Clinical local frequency	No local frequency	p-value
500	6.5 ± 0.2	6.7 ± 0.3	0.2
750	6.4 ± 0.4	8.8 ± 0.2	0.003
1050	5.6 ± 0.3	10.2 ± 0.7	0.003
p-value	<0.02 (wrt 1050 Hz)	0.04	–

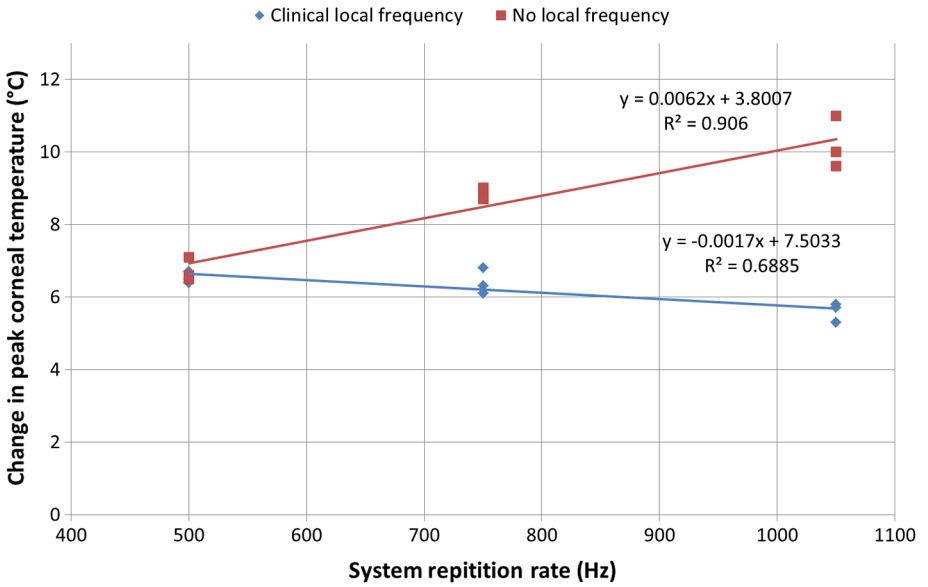

Fig. 5 The change in peak corneal temperature with respect to the system repetition rate. The differences between the two local frequencies became more significant with increasing repetition rate ($p = 0.003$ for 1050-Hz repetition rate), peaking up to 6.8°C for the clinical local frequency.

local frequency was increased to 80 Hz in accordance with the pulse energy control of the local frequency. Therefore, the two tested local frequencies are represented as controlled (80 Hz) and no local frequencies (1000 Hz) in Fig. 7. For both the local frequencies, the differences between the two pulse energy levels were statistically significant ($p = 0.01$ for controlled local frequency and $p = 0.03$ for no local frequency, Table 5). The differences between the two local frequencies increased with increasing pulse energy (Fig. 7), with the change in peak corneal temperature decreasing for higher pulse energy with the controlled local frequency, and increasing for no local frequency. For the controlled local frequency, the highest change in peak corneal temperature was limited to 6.85°C for both the tested pulse energy settings, however, it reached as high as 11°C for no local frequency.

3.5 *Refractive Correction*

Myopic (−9, −6, and −3 D) and hyperopic ablations (+2, +4, and +6 D) were performed with clinical and no local frequency each. The change in peak corneal temperature was significantly higher for myopic corrections in comparison to hyperopic corrections for both the local frequencies ($p = 0.001$ and $p = 0.000009$ for clinical and no local frequency, respectively) (Table 6). The differences between the local frequencies were stable and significant for all the refractive corrections, favoring the clinical local frequency peaking at 6.1°C but reaching up to 9.4°C for no local frequency (Fig. 8).

Table 4 Thermal response to changing OZ size. For both local frequencies, significant differences were observed between the three OZs. The measurements at clinical local frequency were significantly lower compared to no local frequency for the entire range of tested OZ sizes.

OZ (mm)	Clinical local frequency	No local frequency	*p*-value
4	4.4 ± 0.1	12.0 ± 0.1	0.0001
6.3	5.6 ± 0.3	10.2 ± 0.7	0.003
7.5	6.4 ± 0.2	8.6 ± 0.3	0.0002
p-value	0.02	0.02	–

3.6 *Effect of Epithelium*

Transepithelial and stromal ablations were performed with both clinical and no local frequency. For both local frequencies, the change in peak corneal temperature was significantly higher for transepithelial ablations compared to stromal ablations (mean 0.9°C higher, $p < 0.007$ for clinical local frequency and mean 1.3°C higher, $p < 0.1$ for no local frequency). However, the change in peak corneal temperature was similar for the two stromal ablations ($p = 0.3$ for clinical and $p = 0.1$ for no local frequency). Between the two local frequencies, the differences were significant for all corneal ablations ($p < 0.003$) (Table 7).

4 Discussion

The analysis of our results revealed the thermal response of the cornea to varying test parameters with and without the local frequency controls. In our experiments, we set −9 D refractive correction as our basis since nowadays it may be considered as a rather high correction. The clinical local frequency of 40 Hz was specified based on the available literature,[30] and is also being used as a standard value in the AMARIS platform. The no local frequency of 1000 Hz was specified since for a 1050-Hz system repetition rate, this represents no local frequency controls with almost every pulse (9 out of 10 pulses) delivered with 1050-Hz frequency and minimal pulses (1 out of 10 pulses) delivered with 525-Hz frequency. The system repetition rate of 1050 Hz is the highest available repetition rate among excimer laser systems, to the best of our knowledge. The OZ size of 6.3 mm may be considered as the standard clinical value in refractive surgery. A pulse energy level of 1.33 mJ was specified as a standard value for AMARIS high fluence. Paired single

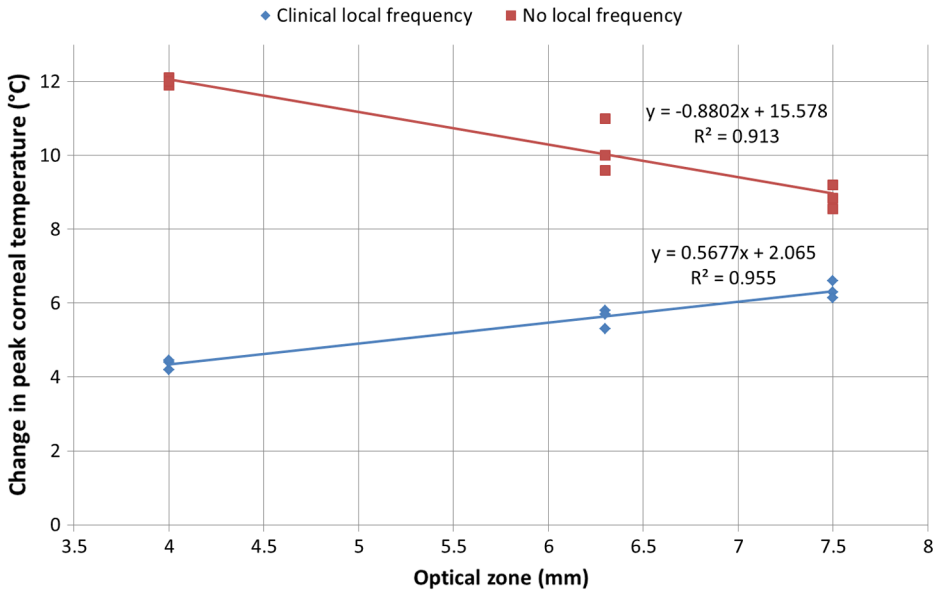

Fig. 6 The change in peak corneal temperature with respect to the optical zone (OZ) sizes. A converging trend is observed between the two local frequencies with increasing OZ sizes. The maximum change in peak corneal temperature (6.6°C) with clinical local frequency was obtained for a 7.5-mm OZ.

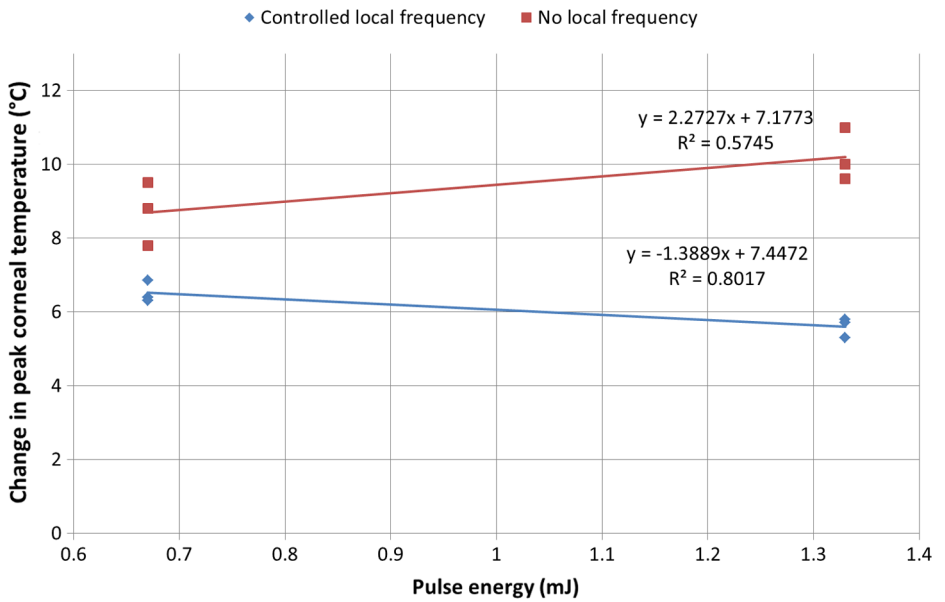

Fig. 7 The change in peak corneal temperature with respect to the pulse energy. The clinical local frequency of 40 Hz was maintained for 1.33-mJ pulse energy, but for half the pulse energy the local frequency was increased to 80 Hz. However, with the controlled local frequency of 80 Hz at 0.67-mJ pulse energy, the maximum change in peak corneal temperature reached up to 6.85°C.

tailed *t*-tests were preferred compared to other statistical tests, such that for each varying parameter, each tested value could be individually compared to all the other tested values. The specific varying parameter and its corresponding impact are discussed as follows:

4.1 *Local Frequency*

The lower range of local frequency (10 Hz) was specified to restrict the radiation power density (number of pulses per unit of time and area) below the clinically used values. Our results showed a logarithmic relationship between the changes

Table 5 Thermal response to changing pulse energy. The pulse energy levels showed significant differences for the two local frequencies. Between the two local frequencies the differences became more significant with increasing pulse energy.

Energy (mJ)	Clinical local frequency	No local frequency	*p*-value
0.67	6.5 ± 0.3	8.7 ± 0.9	0.003
1.33	5.6 ± 0.3	10.2 ± 0.7	0.01
p-value	0.01	0.03	–

Table 6 Thermal response to changing refractive correction. More significant differences showed between myopes and hyperopes for the no local frequency versus the clinical local frequency. For all refractive corrections, the clinical local frequency was favorable in terms of thermal control.

Refraction (D)	Ablation depth (μm)	Clinical local frequency	No local frequency	*p*-value
−9	136.3	5.8 ± 0.2	9.2 ± 0.3	0.00008
−6	90.6	6.0 ± 0.1	8.7 ± 0.4	0.001
−3	45.0	5.2 ± 0.1	8.2 ± 0.5	0.004
+2	32.0	4.4 ± 0.3	7.3 ± 0.6	0.002
+4	69.6	5.0 ± 0.2	7.3 ± 0.8	0.01
+6	111.6	5.2 ± 0.4	6.7 ± 0.5	0.03
p-value myopes versus hyperopes	–	0.001	0.000009	–

in peak corneal temperature with increasing local frequency. These results correspond well with the theoretical predictions. Lowering the local frequency results in improved thermal control, although at the cost of an increment in treatment times and potential hydration losses.

4.2 *Repetition Rate*

The other tested system repetition rates (500 and 750 Hz) are available on older AMARIS versions and also represent a factor of approximately 1/2 and 1/square root (2) of 1050 Hz, providing a wide testing range. For the no local frequency, the change in peak corneal temperature increased linearly ($r^2 = 0.90$) with the increasing system repetition rate, peaking at 1050 Hz (11°C). However, for clinical local frequency, the change in peak corneal temperature was comparatively flat ($r^2 = 0.68$ with a range of 1.5°C), corresponding well with the theoretical predictions.

Table 7 Role of epithelium in thermal control. For both local frequencies, the average change in peak corneal temperature was significantly higher for transepithelial ablations versus intrastromal ablations. The clinical local frequency was again favorable in terms of thermal control, in comparison to no local frequency, with the differences slightly increasing with deeper corneal ablations.

Ablation	Clinical local frequency	No local frequency	*p*-value
Transepithelial	7.0 ± 0.2	10.8 ± 0.4	0.003
1st stromal	6.1 ± 0.3	9.7 ± 0.2	0.002
2nd stromal	6.0 ± 0.1	9.3 ± 0.2	0.001
p-value versus transepithelial	<0.007	<0.01	–

4.3 *Optical Zone*

The OZ of 7.5 mm may be considered as the upper boundary value in refractive surgery. The lower boundary of 4-mm OZ was selected to force the radiation power density much higher than the clinically used values. For the no local frequency, the change in peak corneal temperature decreased linearly ($r^2 = 0.91$) with the increasing OZ size, peaking at 4-mm OZ (12.1°C). However, for the clinical local frequency, the change in peak corneal temperature increased linearly ($r^2 = 0.95$) with the increasing OZ, with a range of 2.4°C. These

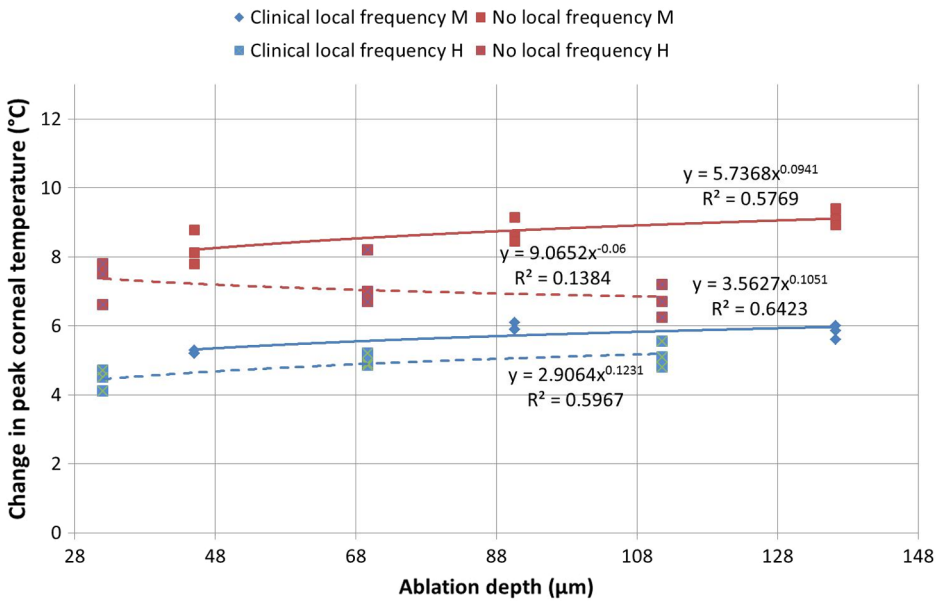

Fig. 8 The change in peak corneal temperature with respect to the ablation depth. Here M and H represent myopic and hyperopic corrections, respectively. Also the ablation depth of 136.3, 90.6, 45.0, 32.0, 69.6, and 111.6 (in μm) correspond to refractive correction of −9, −6, −3, +2, +4, and +6 diopters, respectively. A significantly higher peak corneal temperature was observed for myopic corrections compared to hyperopic corrections, for both the local frequencies, peaking to 6.1°C for clinical local frequency.

results correspond well with the theoretical predictions. For no local frequency, since the pulse density decreases for a wider OZ, there is a higher random chance to hit a cooler corneal region. Additionally, with the clinical local frequency, as the pulse density is highest for the smallest OZ, the local frequency controls act more often, optimizing the thermal load on the cornea.

4.4 *Pulse Energy*

A pulse energy level of 0.67 mJ was specified as a standard value for AMARIS low fluence, representing a factor of 2 in the overall range covered. Laser systems with up to ~2-mJ pulse energy are available,[35] however, such a high metric has not been covered in our tests and related extrapolations based on our results should be made with caution, although 1.33 mJ of pulse energy in a 0.54-mm spot size represents the upper limit of energy density (~500 mJ/cm^2) in refractive surgery. A maximum change in peak corneal temperature of 6.85°C and a range of 1.55°C were observed with the controlled local frequency. These results correspond with the theoretical predictions showing a rather flat decrease in peak corneal temperature with the increasing pulse energy with controlled local frequency since stronger thermal controls are enforced at 1.33-mJ pulse energy with 40-Hz local frequency compared to 0.67-mJ pulse energy with 80-Hz local frequency. Conversely, with no local frequency, the peak corneal temperature increases steadily ($r^2 = 0.57$) with increasing pulse energy.

4.5 *Refractive Correction*

The range of tested refractive correction (−9 to +6 D) represents the standard limits in refractive surgery very well. A significantly higher peak corneal temperature was observed for myopic corrections compared to hyperopic corrections for both the local frequencies. However, the results favored the clinical local frequency with a maximum change in peak corneal temperature of 6.1°C and a range of 2°C for the entire range of refractive correction. These results could be expected, since the local pulse density is higher in the center for myopic corrections, but is lower and disseminating over a peripheral ring for hyperopic corrections.

4.6 *Effect of Epithelium*

With the transepithelial and stromal ablations we could simulate a comparison of thermal effects between transepithelial PRK, thin flap and thick flap laser-assisted *in situ* keratomileusis. The transepithelial ablations resulted in a significantly higher increase in peak corneal temperature compared to the stromal ablations for both the local frequencies. The two stromal ablations, performed at different ablation depths within the stroma, however, gave almost identical results. Our results correspond with the expected ~1°C to 2°C higher transepithelial thermal response as predicted by theoretical models.[34] It is expected that the role of epithelium as a protective outer most layer of the cornea (besides the tear film) results in a higher response to the implied energy in the form of laser pulses, in comparison to the deeper layers of the cornea. However, the average change in peak corneal temperature was 7°C ± 0.2 for transepithelial ablations with clinical local frequency and 10.8°C ± 0.4 for no local frequency, again favoring the local frequency controls.

Our analysis favors the local frequency controls through the entire spectrum of tested parameters. The most extreme rise in peak corneal temperature was 6.85°C (0.67-mJ pulse energy, 1050-Hz system frequency, −9 D refractive correction, 6.3-mm OZ) for clinical local frequency and 12°C (1.33-mJ pulse energy, 1050-Hz system frequency, −9 D refractive correction, 4-mm OZ) for no local frequency. The results presented here corresponded well ($r^2 = 0.789$) with the values achieved from the theoretical model presented elsewhere[34] (Fig. 9). These results suggest that the entire spectrum of tested parameters with the clinical local frequency of 40 Hz lie in a comfortable range to avoid any thermal damage during ablation, contrary to the results with no local frequency of 1000 Hz. The thermal load problem in refractive surgery in relation to the frequency controls has been explored by many researchers and commercial platforms in the past.[11,36–38] Our results suggest that increasing

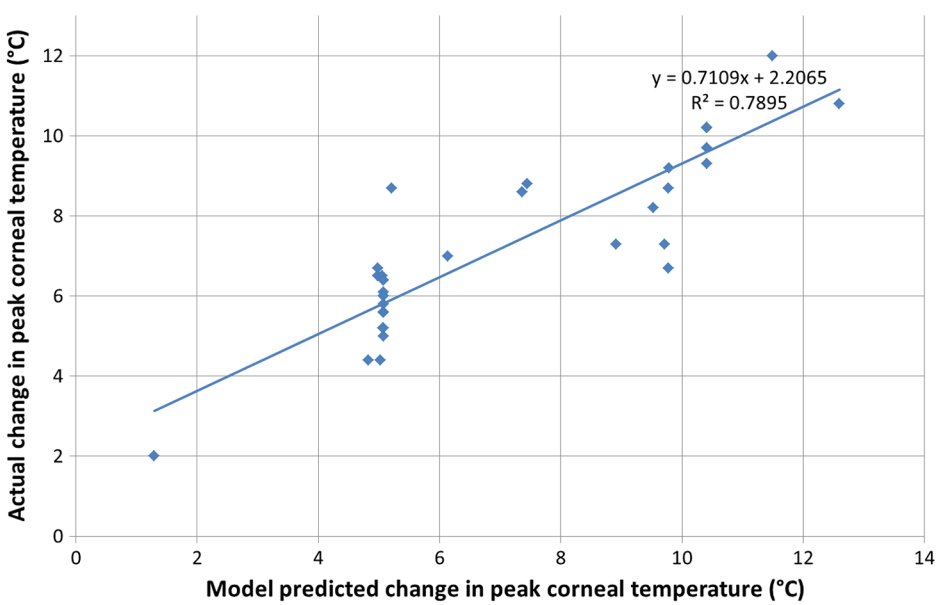

Fig. 9 A comparison of the achieved change in peak corneal temperature versus the model predicted values for the corresponding settings.

the local frequency beyond 80 Hz for a refractive surgery planned with an OZ beyond 6.3 mm for a high-refractive correction (for example −9 D) could lead to a change in peak corneal temperature beyond 10°C, leading to potential thermal damage.[11,30,31] Furthermore, the difference between the epithelial and stromal thermal response to ablation (~1.2°C higher for epithelium) shines light on the thermal safety control of transepithelial and stromal refractive procedures. The role of epithelium in corneal thermal response must be considered while planning refractive surgeries based on transepithelial ablations, in addition to the considerations of epithelial thickness profile versus the applied epithelial ablation profiles.[39] These results could be extended to clinics for planning safer refractive procedures considering the association between human and porcine eyes.[20] Since the tested parameters are inter-related for refractive surgery planning and laser system specifications, our recommendation covers many of these parameters together. Individually, the impact of each parameter on the change in peak corneal temperature beyond a safe limit is reflected in Tables 2–7.

Mrochen et al.[11] performed a similar study with bovine eyes with an aim to investigate the influence of temporal and spatial spot sequences on the OST increase during corneal laser surgery. They recorded the increase in the corneal temperature for various refractive corrections and temporal distribution of ablation profiles (4 spot sequences: line, circumferential, random, and an optimized scan algorithm) using an IR camera. They found that the highest maximum temperature increases were observed with the line and circumferential scans and the lowest with the random and optimized scans. In addition, the temporal scan dependence, the type of ablation (myopic, hyperopic, or PTK) influenced the maximum temperature measured, with the myopic corrections showing a much higher increase in corneal temperature compared to hyperopic corrections. This relation was also observed in our results for both the tested local frequencies. However, we reported a much lower change in peak corneal temperature with the clinical local frequency for the same refractive correction compared to their optimized scan algorithm allowing a spot positioning with a maximum local frequency of 200 Hz at each point of the treatment zone.

Other studies, however, also undermine the impact of ablation frequency regarding their clinical side effects. Khoramnia et al.[40] evaluated the effect of three excimer laser ablation frequencies (200, 500, and 1000 Hz) on the cornea using a 1000-Hz scanning-spot excimer laser and found no specific side effects associated with the high-repetition rates based on structural and ultrastructural evaluation of corneas. The ablation quality was comparable in the three frequency groups with the fastest treatment times with 1000 Hz. Similar findings were reported by Shanyfelt et al.,[41] between corneal ablation profiles created at 60 and 400 Hz, with an average rate of 0.94 μm/pulse at 60 Hz versus 0.92 μm/pulse at 400 Hz.

Betney et al.[42] used a matrix of 10×10 pixels within an area of 1 cm^2 at the center of the cornea to evaluate the maximum temperature. They found that mean (±SD) central OST after epithelial debridement was 29.15 ± 0.39°C. Mean peak OST during PRK was 37.77 ± 0.67°C, with most of the temperature increase occurring during the first 15 s. Pattmöller[43] analyzed the corneal surface temperature profile in a young and healthy study population to determine the impact of corneal thickness, anterior chamber depth, and endothelial cell density on surface temperature. They analyzed 61 healthy right eyes of 61 subjects without tear film pathologies (mean age 24.9 ± 6.7 years). They found no correlation between OST and corneal thickness, anterior chamber depth or endothelial cell density. On average, local OST was highest at measurement positions where corneal thickness was lowest, but without reaching statistical significance. Baseline OST was highest at thin corneal regions and temperature decay over time was smallest in those regions. They concluded that the general temperature profile seems to be influenced by the corneal thickness profile resulting in a higher temperature and lower decay at thinner corneal regions.

An extensive review of the methods of ocular temperature distribution measurement was presented by Ooi and Ng.[12] They presented a comparison of the mathematical modeling approach with the IR thermography methods. Bioheat equations accompanied by boundary conditions are usually used to describe the heat transfer phenomena inside the eye and mathematically model the physical phenomena. Ooi et al.[44] presented a three-dimensional (3-D) radially symmetric boundary element model of the human eye for simulating changes in corneal temperature during treatment of laser thermokeratoplasty. They modeled the energy absorption inside the cornea using the Beer–Lambert law. They solved the resulting initial-boundary value problem numerically using a time-stepping boundary element method. They calculated the temperature field for heating by both the pulsed laser and the continuous wave laser. Nga et al.[45] presented a comparative study between the two-dimensional (2-D) and 3-D human eye models. Their comparisons between the temperatures at various points inside the human eye suggested that for some initial investigations, the use of a 2-D model may be sufficient. However, in other cases such as the loss of thermal symmetry (asymmetrical boundary conditions, power deposition inside the eye), the use of a 3-D model is preferable.

The use of a literature based emissivity factor may be termed as a limitation of this study. In addition, the relation between the tilt of the camera and the curvature in the cornea surface could occlude or hinder some part of the cornea during measurement; however, it was cautiously controlled during manual adjustment of the camera. Additionally, the use of rotationally symmetric profiles should compensate for this. We did not test the thermal impact of rotationally nonsymmetric profiles, but the laser tissue interaction should result in a similar thermal impact using such profiles.

OST has been shown to vary topographically.[46,47] Also, we must account for the fact that porcine eyes can differ in size, position, and slightly in shape. These differences in full 3-D should be properly accounted for in 2-D thermal image analysis. Our group[20] previously analyzed this issue in a case study on the porcine eye 2-D temperature distributions with a lateral resolution of 170 μm and line scans with a temporal resolution of 13 μs. The gray-level coded temperature values belonging to pixels in the center of the ablation zone (lying inside the calibrated area) were analyzed. Outside the calibrated area, the temperature was assumed to not only be altered due to the laser ablation profile, but also due to the curvature of the porcine eyes. Within the calibrated inner areas, one of the lines clearly showed a hot spot. In our current test setup, we selected −9 D correction for the majority of treatments, which has a clear central max depth, so the pixel position with the max temperature tends to be close to the center with a known and controlled angle projection. However, the hyperopic corrections might be more sensitive to these subtle differences.

Another weakness was due to the limitation in manipulating our test software for the pulse energy control of the local

frequency. Under the influence of local frequency control, a change in laser pulse energy manipulated the local frequency in order to maintain a constant fluence received by the eye per unit of time. This control was deactivated for "no local frequency." For the tests concerning the impact of pulse energy on change in peak corneal temperature, under local frequency controls the clinical local frequency of 40 Hz could not be maintained for a pulse energy of 0.67 mJ. In an ideal case, the impact of the pulse energy should be explored maintaining similar local frequency controls; however, our test software did not easily allow this freedom.

Although we tested the extremities of each parameter technically feasible with our setup, extrapolation of our results beyond these limits must be done with caution. Furthermore, the measurement was updated at every third to fifth laser pulse depending on the system repetition rate (with no local frequency) in comparison to the acquisition rate of the camera. However, with the local frequency controls (clinical local frequency), the acquisition rate of the camera was comparatively much higher. This means that the tested local frequencies of ablation (clinical and no local frequency) for different system repetition rates were, in some cases, much higher, and in other cases much lower than the frame rate (200 Hz) of the camera. We had the liberty to choose between different frame rates (in windowed mode) with the thermal camera used in our test setup. The frame rate also affected the size of the acquisition window, with a higher frame rate allowing a smaller acquisition window. Our choice was based on the largest acquisition window compatible with the fastest frame rate, then the working distance was selected to offer a window large enough to comfortably cover the limbus in the porcine eyes (with some room for variability in the eyes), and from that the observation angle has been selected as the most vertical line that did not interfere with the laser contour. We used the same frame rate with different local frequencies to maintain conformity within our test setup and because the (limited) available acquisition rates could not be correlated with all the different parameter choices.

Due to the vastly different time scales (nanoseconds for the laser pulses, milliseconds for the camera frame rate), the resulting thermal images contain information that is integrated or averaged in time. However, our interest was to measure the temperature of the remaining cornea as opposed to the dynamics of the ejected and ablated tissue, hence the "slow time domain" (averaging/integrating) helps us to get closer to the biological effects on the residual stroma.

The dynamics of the temperature change during the ablation process could also be a relevant factor and were not analyzed in this study. The extrapolation of these results based on postmortem pig eyes to human eyes could be affected by the condition of the pig eyes. However, eyes with cloudy corneas likely affected in biomechanics and functionality were avoided in our experiments.

The presented results reiterate the dilemma in refractive surgery development. Using controlled local frequency settings maintains a safe thermal load at the cornea but at the cost of increased treatment times. This can eventually affect the hydration of the corneal surface during the treatment.[48] The corneal hydration reduces with increasing treatment times, affecting the ablation properties on the cornea, indicating a preference for a faster treatment. However, increasing the local frequency beyond a certain limit ensures faster treatments, but at the risk of denaturation of the corneal tissue. In addition to these factors, the benefits of transepithelial refractive procedures must be evaluated against the additional increase in corneal temperature compared to stromal refractive procedures. A delicate balance needs to be maintained to achieve optimum ablation efficiency in coherence with safer thermal controls.

Acknowledgments

This article has not been presented at any meeting. The authors did not receive any financial support from any public or private sources. They have no financial or proprietary interest in a product, method, or material described herein, but they both are employees of SCHWIND eye-tech-solutions. This article represents the personal views of the authors and was not written as a work for hire within the terms of the authors' employment with SCHWIND eye-tech-solutions. They acknowledge Mr. Bastian Bratenstein (SCHWIND eye-tech solutions) for his support in conducting the experiments. The work described in this article itself (as opposed to the work done writing the article) was conducted as part of their work for SCHWIND eye-tech-solutions. Content attributed to the authors was vetted by the standard SCHWIND eye-tech-solutions approval process for third-party publications.

References

1. S. Arba-Mosquera and T. Klinner, "Improving the ablation efficiency of excimer laser systems with higher repetition rates through enhanced debris removal and optimized spot pattern," *J. Cataract Refractive Surg.* **40**(3), 477–484 (2014).
2. M. Mrochen et al., "Influence of spatial and temporal spot distribution on the ocular surface quality and maximum ablation depth after photoablation with a 1050 Hz excimer laser system," *J. Cataract Refractive Surg.* **35**(2), 363–373 (2009).
3. J. D. Gottsch et al., "Excimer laser calibration system," *J. Refractive Surg.* **12**(3), 401–411 (1996).
4. S. Arba-Mosquera and S. Verma, "Analytical optimization of the ablation efficiency at normal and non-normal incidence for generic super Gaussian beam profiles," *Biomed Opt. Express* **4**, 1422–1433 (2013).
5. J. R. Jiménez et al., "Effect on laser-ablation algorithms of reflection losses and nonnormal incidence on the anterior cornea," *Appl. Phys. Lett.* **81**, 1521 (2002).
6. J. Morelli et al., "Ultraviolet excimer laser ablation: the effect of wavelength and repetition rate on in vivo guinea pig skin," *J. Invest. Dermatol.* **88**(6), 769–773 (1987).
7. M. Ishihara et al., "Temperature measurement for energy-efficient ablation by thermal radiation with a microsecond time constant from the corneal surface during ArF excimer laser ablation," *Front. Med. Biol. Eng.* **11**(3), 167–175 (2001).
8. M. Ishihara et al., "Measurement of the surface temperature of the cornea during ArF excimer laser ablation by thermal radiometry with a 15-nanosecond time response," *Lasers Surg. Med.* **30**, 54–59 (2002).
9. M. Ishihara et al., "Assessment of expressions of heat shock protein (HSP 72) and apoptosis after ArF excimer laser ablation of the cornea," *J. Biomed. Opt.* **9**(1), 187–192 (2004).
10. F. Brygo et al., "Laser heating and ablation at high repetition rate in thermal confinement regime," *Appl. Surf. Sci.* **252**, 8314–8318 (2006).
11. M. Mrochen et al., "Effect of time sequences in scanning algorithms on the surface temperature during corneal laser surgery with high-repetition-rate excimer laser," *J. Cataract Refractive Surg.* **35**(4), 738–746 (2009).
12. E. H. Ooi and E. Y. K. Ng, "Ocular temperature distribution: a mathematical perspective," *J. Mech. Med. Biol.* **09**, 199 (2009).
13. C. Purslow and J. S. Wolffsohn, "Ocular surface temperature," *Eye Contact Lens* **31**, 117–123 (2005).
14. R. Mapstone, "Determinants of corneal temperature," *Br. J. Ophthalmol.* **52**(10), 729–741 (1968).

15. R. Mapstone, "Normal thermal patterns in cornea and periorbital skin," *Br. J. Ophthalmol.* **52**(11), 818–827 (1968).
16. R. Mapstone, "Corneal thermal patterns in anterior uveitis," *Br. J. Ophthalmol.* **52**(12), 917–921 (1968).
17. J. H. Tan et al., "Infrared thermography on ocular surface temperature: a review," *Infrared Phys. Technol.* **52**, 97–108 (2009).
18. J. Bodycomb et al., "Thin film and emissivity effects on radiometric temperature measurement accuracy," in *RTP2003*, pp. 117–123 (2003).
19. D. J. Hatcher and J. A. D'Andrea, "Effects on thermography due to the curvature of the porcine eye," in *InfraMation*, Naval Health Research Center Detachment, Brooks, Texas (2003).
20. U. Brunsmann et al., "Evaluation of thermal load during laser corneal refractive surgery using infrared thermography," *Infrared Phys. Technol.* **53**, 342–347 (2010).
21. J. M. Kim et al., "Effect of thermal preconditioning before excimer laser photoablation," *J. Korean Med. Sci.* **19**(3), 437–46 (2004).
22. C. Maldonado-Codina, P. B. Morgan, and N. Efron, "Thermal consequences of photorefractive keratectomy," *Cornea* **20**(5), 509–515 (2001).
23. D. De Ortueta et al., "In vivo measurements of thermal load during ablation in high-speed laser corneal refractive surgery," *J. Refractive Surg.* **28**(1), 53–58 (2012).
24. M. Vetrugno et al., "Corneal temperature changes during photorefractive keratectomy using the Laserscan 2000 flying spot laser," *J. Refractive Surg.* **17**(4), 454–459 (2001).
25. J. Wernli et al., "Initial surface temperature of PMMA plates used for daily laser calibration affects the predictability of corneal refractive surgery," *J. Refractive Surg.* **28**(9), 639–644 (2012).
26. N. Efron, G. Young, and N. A. Brennan, "Ocular surface temperature," *Curr. Eye Res.* **8**(9), 901–906 (1989).
27. R. Mapstone, "Measurement of corneal temperature," *Exp. Eye Res.* **7**, 237–243 (1968).
28. P. Rysä and J. Savaranta, "Thermography of the eye during cold stress," *Acta Ophthalmol. Suppl.* **123**, 234–239 (1974).
29. J. P. Craig et al., "The role of tear physiology in ocular surface temperature," *Eye* **14**, 635–641 (2000).
30. T. Bende, T. Seiler, and J. Wollensak, "Side effects in excimer corneal surgery, corneal thermal gradients," *Graefes Arch. Clin. Exp. Ophthalmol.* **226**, 277–280 (1988).
31. M. Lewis, M. Dubin, and V. Aandahl, "Physical properties of bovine corneal collagen," *Exp. Eye Res.* **6**, 57–69 (1967).
32. S. A. Mosquera and M. Shraiki, "Analysis of the PMMA and cornea temperature rise during excimer laser ablation," *J. Mod. Opt.* **57**, 400–407 (2010).
33. U. Brunsmann et al., "Minimisation of the thermal load of the ablation in high-speed laser corneal refractive surgery: the 'intelligent thermal effect control' of the AMARIS platform," *J. Mod. Opt.* **57**, 466–479 (2010).
34. M. Shraiki and S. Arba-Mosquera, "Simulation of the impact of refractive surgery ablative laser pulses with a flying-spot laser beam on intra-surgery corneal temperature," *Invest. Ophthalmol. Visual Sci.* **52**(6), 3713–3722 (2011).
35. M. Mrochen et al., "Experimental setup to determine the pulse energies and radiant exposures for excimer lasers with repetition rates ranging from 100 to 1050 Hz," *J. Cataract Refractive Surg.* **35**(10), 1806–1814 (2009).
36. "Brochure MEL 90 from Zeiss Meditec," http://meditec.zeiss.com/content/dam/Meditec/downloads/pdf/ESCRS/czm_Broschure_MEL90.pdf.
37. C. Winkler von Mohrenfels et al., "First clinical results of epithelial laser in situ keratomileusis with a 1000 Hz excimer laser," *J. Cataract Refractive Surg.* **36**(3), 449–455 (2010).
38. G. D. Kymionis et al., "Effect of excimer laser repetition rate on outcomes after photorefractive keratectomy," *J. Cataract Refractive Surg.* **34**(6), 916–919 (2008).
39. S. A. Mosquera and S. T. Awwad, "Theoretical analyses of the refractive implications of transepithelial PRK ablations," *Br. J. Ophthalmol.* **97**(7), 905–911 (2013) Epub 2013 Apr 20.
40. R. Khoramnia et al., "Effect of 3 excimer laser ablation frequencies (200 Hz, 500 Hz, 1000 Hz) on the cornea using a 1000 Hz scanning-spot excimer laser," *J. Cataract Refractive Surg.* **36**(8), 1385–1391 (2010).
41. L. M. Shanyfelt et al., "Effects of laser repetition rate on corneal tissue ablation for 193-nm excimer laser light," *Lasers Surg. Med.* **40**(7), 483–493 (2008).
42. S. Betney et al., "Corneal temperature changes during photorefractive keratectomy," *Cornea* **16**, 158–161 (1997).
43. J. Pattmöller et al., "Correlation of corneal thickness, endothelial cell density and anterior chamber depth with ocular surface temperature in normal subjects," *Z Med. Phys.* (2014).
44. E. H. Ooi, W. T. Ang, and E. Y. Ng, "A boundary element model for investigating the effects of eye tumor on the temperature distribution inside the human eye," *Comput. Biol. Med.* **39**(8), 667–677 (2009).
45. E.-Y.-K. Nga, E.-H. Ooia, and U. R. Archaryab, "A comparative study between the two-dimensional and three-dimensional human eye models," *Math. Comput. Modell.* **48**(5–6), 712–720 (2008).
46. P. B. Morgan et al., "Potential applications of ocular thermography," *Optom. Vision Sci.* **70**(7), 568–576 (1993).
47. J. H. Tan, E. Y. K. Ng, and U. R. Acharya, "Evaluation of Topographical Variation in Ocular Surface Temperature by Functional Infrared Thermography," *Infrared Phys. Technol.* **54**(6), 469–477 (2011).
48. D. de Ortueta et al., "Influence of stromal refractive index and hydration on corneal laser refractive surgery," *J. Cataract Refractive Surg.* **40**(6), 897–904 (2014).

Samuel Arba Mosquera received his PhD in sciences of vision from the University of Valladolid in 2007 to 2012 and physics from the University of Santiago de Compostela in 1993 to 1998. He works as an optical/visual researcher at SCHWIND eye-tech-solutions (Germany), with fifteen years of experience in R&D in optics and vision and expertise in development of algorithms for refractive surgery.

Shwetabh Verma received his MSc degree in biomedical optics engineering from the Ruprecht Karls University Heidelberg, Germany, with a visiting research scholarship with Shiley Eye Center UC, San Diego. Currently, he is associated with the R&D Department of SCHWIND eye-tech-solutions, Germany, as a biomedical optics engineer. His recent published work and current research interests include super Gaussian beam profiles, cyclotorsion compensation, eye tracking and prediction models, and refractive surgery optimization algorithms.